

Microporous N-doped Carbon Electrochemical Catalyst Derived from Polyacrylamide Hydrogel for Oxygen Reduction Reaction in Alkaline Media

Ming Chen¹, Rui Wang², Shichang Cai², Ping Mei¹, Xuemin Yan^{1,*}, Yu Jiang¹, Yan Zhang¹, Wei Xiao¹, Haolin Tang^{2,*}

¹ College of Chemistry and Environmental Engineering, Yangtze University, Jingzhou, 434023, Hubei, P. R. China.

² State Key Laboratory of Advanced Technology for Materials Synthesis and Processing, Wuhan University of Technology, Wuhan, 430070, Hubei, P. R. China.

*E-mail: XueminYan@126.com, thln@whut.edu.cn

Received: 11 November 2017 / Accepted: 13 January 2018 / Published: 5 February 2018

In this work, a series of nitrogen-doped microporous carbon materials with varying N/C ratios have been synthesized by direct carbonization of polyacrylamide hydrogel. The N/C atomic ratios can be accommodated by regulating the amount of urea during the preparation of the hydrogel, and the final microporous structures are obtained after KOH activation. These materials present high oxygen reduction reaction (ORR) activities in alkaline electrolytes, and the ORR performance of such materials is highly dependent on the N/C atomic ratio of precursors. Among these catalysts, the sample labeled PAM-N-0.41 displayed better ORR catalytic performance and stability than commercial Pt/C catalysts. The excellent ORR performance of PAM-N-0.41 can be attributed to its high specific surface area and large numbers of exposed active sites derived from the doping of nitrogen.

Keywords: oxygen reduction reaction; electrochemical catalyst; microporous nitrogen-doped carbon; polyacrylamide hydrogel

1. INTRODUCTION

There is increasing demand for clean and sustainable energy conversion systems due to the limited availability of fossil fuels and growing environmental concerns; these systems include fuel cells and metal-air batteries[1-3]. However, the practical application of these energy technologies in real life remains a challenge due to the sluggish kinetics of the oxygen reduction reaction (ORR), which is the main electrochemical reaction occurring at the cathode of such devices[4]. In recent decades, Pt-based electrocatalysts have emerged as the most effective materials towards the ORR, and

their corresponding development has attracted extensive and intensive research[5]. However, the high price and relatively poor durability of Pt catalysts have hindered the further commercialization of these materials[6]. Therefore, numerous studies have been conducted for the development of low-cost and high-performance non-Pt electrocatalysts.

To our knowledge, various efforts have been made to reduce or replace Pt-based electrocatalysts with non-precious metal catalysts[7,8], metal alloys[9,10], transition metal compounds[11-13], metal-nitrogen-doped carbon materials[14,15], and metal-free doped carbon materials[16-20]. These materials have proven efficient for the ORR. Among the catalysts mentioned above, nitrogen-doped carbon materials have attracted particular interest, with potential as outstanding ORR electrocatalysts due to their good conductivity, low cost and good endurance[21]. Tremendous work has been done to enhance the ORR performance of nitrogen-doped carbon by adopting suitable precursors and designing appropriate nanostructure[22-28]. These results mainly focus on two crucial factors, which may play important roles in catalyzing ORR performance. One is that doped nitrogen content and type determine the intensity and catalytic ability of the active sites. Generally, nitrogen atoms can be doped into the basal plane of a graphitic carbon sheet in several different configurations (pyridinic, pyrrolic and graphitic nitrogen)[29,30]. These nitrogen configurations can adjust the electronic properties of neighbor carbon atoms and thus affect the physical and chemical properties of the catalysts[31]. Although the exact catalytic role for each nitrogen form in carbon materials is still debated, there is no doubt that the ORR performance of nitrogen-doped carbon strongly depends on the type of nitrogen precursors used and the nitrogen content of catalysts. The other is that a porous structure is required for ideal ORR catalysts. The large specific surface/interface areas provided by porous materials can guarantee that the reagents are accessible to active sites and favor efficient electron/electrolyte transport. Accordingly, the higher surface areas of porous nitrogen-doped carbon materials with optimized nitrogen content are highly desirable for ORR catalysts.

Here, we report a facile method for the synthesis of nitrogen-doped microporous carbon materials derived from polyacrylamide hydrogel precursors. The active site number is regulated by controlling the amount urea during hydrogel formation, and porous structures are obtained after KOH activation. The prepared catalysts exhibit excellent performance towards the ORR, which could be attributed to the high specific surface area, abundant microporous channels and optimized nitrogen content doped in the carbon framework.

2. EXPERIMENTAL

2.1. Materials

Acrylamide, N,N'-methylenebisacrylamide (99%), ammonium persulfate, and urea were purchased from Sinopharm Chemical Reagent Co., Ltd. (Shanghai, P.R. China). All reagents were analytically pure and used without further purification.

2.2. Preparation of PAM-N-x catalysts

For polyacrylamide hydrogel synthesis, briefly, 5.0 g acrylamide monomer and 0.005 g N,N'-methylenebisacrylamide (99%) was dissolved in 20 mL deionized water, and 0-1.2 g urea was added. After stirring for ~10 min, 1.0 mL 1.32×10^{-2} M ammonium persulfate solution was added dropwise with stirring. The mixture was placed in a water bath (60 °C) for 2 h to obtain the polyacrylamide hydrogel. For freeze-drying and carbonization, the prepared hydrogel was placed in a vacuum freeze dryer at -30 °C for 3 days, and then the dried sample was pyrolyzed under flowing N₂ at 800 °C with a heating rate of 5 °C min⁻¹ for 2 h. For KOH activation, the carbonized materials were mixed with solid KOH (mass ratio of KOH:carbon = 2:1) and annealed at 750 °C for 2 h under a nitrogen atmosphere with a heating rate of 5 °C min⁻¹. The resulting dark powder was washed with 1 M HCl and deionized water, followed by drying at 80 °C overnight. The synthesized catalysts with varying added urea were labeled PAM-N-x, where the numeric suffix (x) indicates the nominal N/C atomic ratio of each catalyst. This value was calculated considering all N and C atoms in the precursors used for the synthesis of the final catalysts. When the additive urea amounts were 0, 0.3, 0.6, 0.9 and 1.2 g, the value of x was 0.33, 0.37, 0.41, 0.44 and 0.48, respectively.

2.3. Characterization

X-ray powder diffraction (XRD) measurements were performed with a D8 Advance from the Brooke AXS Company (Karlsruhe Germany). The Raman spectra of the samples were recorded using a Raman system (Invia, Renishaw) with an excitation energy of 2.41 eV. X-ray photoelectron spectroscopy (XPS) analysis was performed on a VG Multilab 2000 X-ray photoelectron spectrometer (VG Scientific, Massachusetts, USA). Surface area analysis was performed through liquid nitrogen cryosorption (ASAP 2000, Micromeritics) and the distribution of micropore size was calculated by dynamic function theory (DFT) methods with the adsorption curves. The carbon, nitrogen, and hydrogen contents of the samples were measured with an elemental analyzer (Vario EL cube).

2.4. Electrochemical measurements

The electrochemical properties of the catalysts were characterized using a standard three-electrode configuration. A glassy-carbon electrode (5.00 mm in diameter) served as the working electrode, a Pt black electrode served as the counter electrode, and an RHE electrode served as the reference electrode, respectively. The working electrode was coated with a catalyst ink, which was prepared by ultrasonically stirring 5.0 mg of the catalyst with 900 μL of isopropanol, 100 μL of deionized water, and 20 μL of Nafion solution. 20 μL of the ink was deposited onto the glassy carbon surface to obtain the working electrode. The catalyst loading was calculated as 0.51 mg cm⁻². Cyclic voltammetry (CV) and linear sweep voltammetry (LSV) measurements were performed to evaluate ORR activities. CVs were recorded without rotation in 0.1 M KOH solutions saturated with O₂ gas. LSV measurements were performed by varying the sweeping potential from 0.2 V to 1.1 V vs. RHE with a scan rate of 5 mV s⁻¹. Chronoamperometric testing of all samples was conducted in O₂-saturated

0.1 M KOH (0.6 V vs. RHE) at room temperature. The LSV measurements were collected in O₂-saturated solutions with a rotation speed of 400-2000 rpm. The current density during the electrochemical measurements was calculated from the geometrical area of the electrode (0.196 cm⁻²). Using the RDE results, the number of transferred electrons during the ORR process was determined by the Koutecky–Levich equation.

3. RESULTS AND DISCUSSION

XRD measurement was conducted to study the composition phase of the products. Fig. 1(a) shows the XRD patterns of PAM-N-x with x=0.33-0.48. There are two broad peaks at 26.4° and 43.2° in all the XRD spectra of PAM-N-x. These peaks could be assigned to the (002) and (101) plane of graphite carbon, respectively. The graphitization degree is probed by Raman spectra analysis, and the results are shown in Fig. 1(b). The typical D band (~1300 cm⁻¹) and G band (~1580 cm⁻¹) are observed in the Raman spectra of the catalysts. Generally, G mode arises from first-order scattering of the E2g phonon of sp² C atoms, and D mode is a defect peak arising from intervalley scattering[32]. The I_d/I_g value can reflect the defect degree of materials. As depicted in Figure 1(b), the I_d/I_g values are similar in all catalysts, which indicates that the N/C ratio has almost no significant effect on the degree of graphitization of all samples, in accordance with the XRD results.

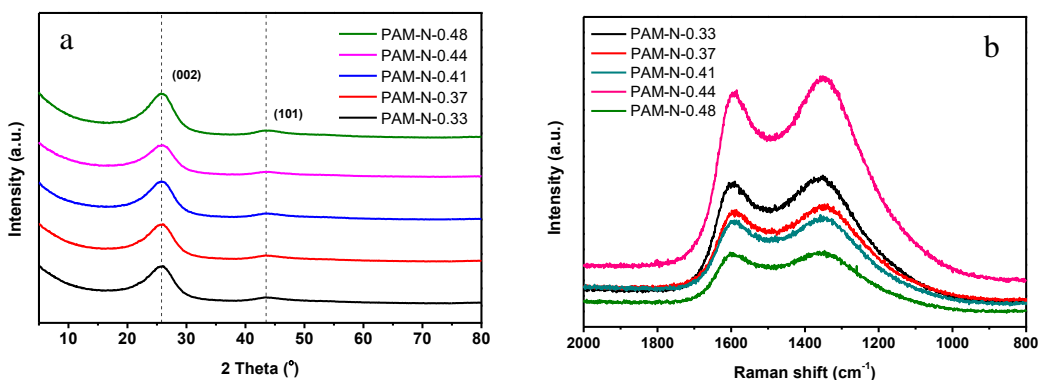


Figure 1. XRD patterns (a) and Raman spectra (b) of PAM-N-x with x=0.33-0.48.

Table 1 shows the H, C and N contents of the N-doped carbon electrocatalysts as detected by elemental analysis. The amount of nitrogen incorporated into the final catalyst increases with increasing urea adding during synthesis. The theoretical and actual N/C values are shown in Table 1. The results indicate that the actual N content in the catalysts is significantly lower than the calculated nominal values. XPS survey spectra for PAM-N-x are shown in Fig. 2 (a). The surface elemental compositions of the PAM-N-x samples corresponding to XPS results are shown in Table 2, which reveals the constituents of the PAM-N-x electrocatalysts as C, N and O. As observed, the surface N/C ratios are increasing with increasing added urea. As expected, PAM-N-0.48 had the highest N content. In addition, as shown in Table 1 and Table 2, the N/C atomic ratios from elemental analyses are higher than the surface N/C atomic ratios obtained by XPS. This indicates that N atoms not only are located at the surface of the catalysts but are also present in the inner layers of the catalysts[33]. For more

detailed information about nitrogen configurations, high-resolution XPS spectra corresponding to the N 1s peaks of PAM-N-x are shown in Fig. 2(b).

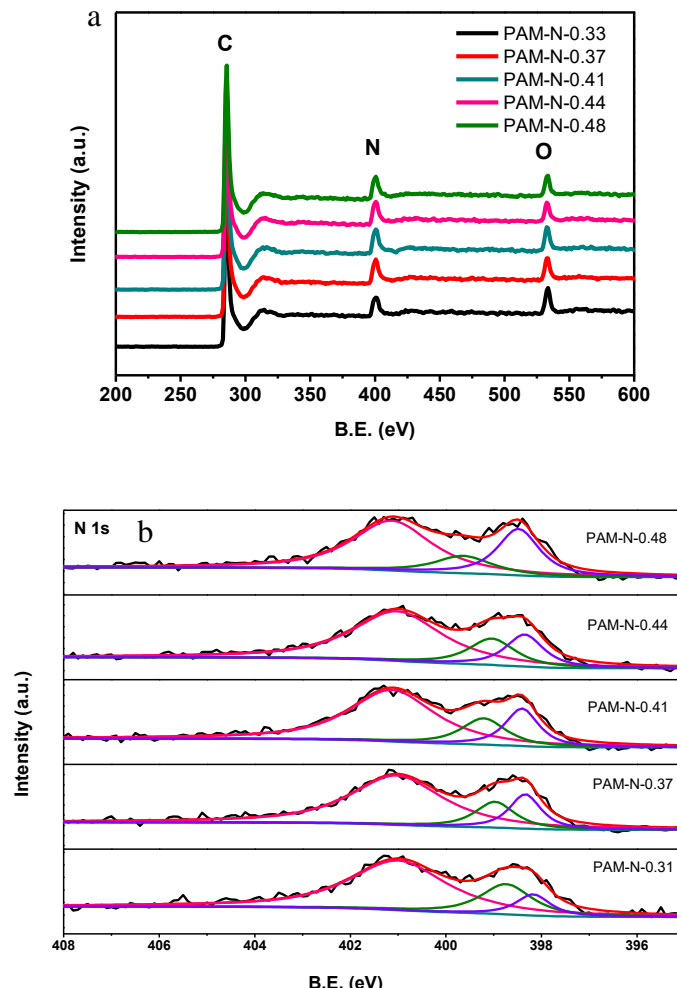


Figure 2. (a) XPS survey spectra of PAM-N-x samples. (b) N 1s core-level spectra of PAM-N-x samples (black line). Peaks for N-pyridinic, N-pyrrolic and N-graphitic are in purple, green, and red, respectively.

Table 1. C, N and H content determined by elemental analysis and N/C weight ratios. Carbon, nitrogen and hydrogen contents were measured with an elemental analyzer; N/C weight ratio and atomic ratio were calculated from test results.

Sample	Weight content (%)			N/C weight ratio	N/C atomic ratio
	C	H	N		
PAM-N-0.33	88.35	0.88	0.89	0.010	0.009
PAM-N-0.37	87.85	0.86	1.98	0.023	0.020
PAM-N-0.41	86.58	0.85	2.45	0.028	0.024
PAM-N-0.44	86.34	0.82	2.62	0.030	0.026
PAM-N-0.48	85.26	0.76	2.86	0.034	0.029

The N 1s spectrum could be deconvoluted into three individual components. These peaks can be assigned to pyridinic N (398.4 eV), pyrrolic N (399.1 eV), and graphitic N (401.2 eV)[6,34],

respectively. In all cases, graphitic N is the most abundant species. For PAM-N-0.33, the relative amounts of pyridinic N and pyrrolic N species are 0.10 and 0.22, respectively. When urea was added as a supplementary N resource during the synthesis, the relative amounts of pyridinic N species increased while the pyrrolic N species declined.

Table 2. N/C surface atomic ratios and relative atomic amount of N species derived from XPS analyses. Textural parameters of samples calculated by N_2 adsorption. Micropore/external area values are shown in brackets.

Sample	Surface N/C Atomic ratios	Relative atomic amount of N species			BET/ $m^2\ g^{-1}$	$V_{\text{micro}}\ (\text{cm}^3\ \text{g}^{-1})$
		Pyridinic N	Pyrrolic N	Graphitic N		
PAM-N-0.33	0.008	0.10	0.22	0.68	2511(1220/1291)	0.65
PAM-N-0.37	0.016	0.16	0.15	0.68	2283(1150/1133)	0.63
PAM-N-0.41	0.020	0.18	0.17	0.65	2022(1055/967)	0.55
PAM-N-0.44	0.023	0.18	0.17	0.65	1822(893/929)	0.48
PAM-N-0.48	0.025	0.28	0.15	0.57	1528(918/610)	0.49

As observed, the relative amounts of pyridinic N and pyrrolic N species either are not altered significantly with further increasing in urea or increase from 0.3 g in PAM-N-0.37 to 0.9 g in PAM-N-0.44. However, when the added urea reached 1.2 g in PAM-N-0.48, the relative amounts of pyridinic N increased to 0.28, and the relative amounts of graphitic N decreased to 0.57, correspondingly.

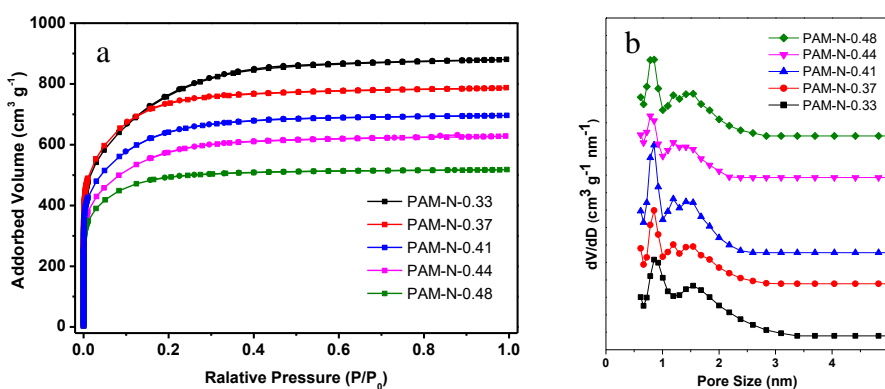


Figure 3. (a) Nitrogen adsorption and desorption curves and (b) pore size distribution of PAM-N-x samples. Distribution of micropore size was calculated using DFT methods with the adsorption curves.

To investigate the pore structure of PAM-N-x samples, nitrogen adsorption and desorption isotherms were conducted at 77 K, and the results are shown in Fig. 3(a). The curves of all samples exhibit a typical Type-I sorption isotherm without hysteresis, indicating the microporous structure of these samples. The specific surface area and pore volume in Table 2 show that the contribution of external area to the total area of all catalysts is significant, irrespective of N/C ratio. With increasing additive urea, the total surface area of PAM-N-x samples fell from 2511 to 1528 $\text{m}^2 \text{ g}^{-1}$. Fig. 3(b) illustrates the pore size distribution (PSD) curves of all samples. The PSDs of PAM-N-x are mainly centralized in the microporous region (0–2.0 nm), with a sharp peak at 0.74 nm and a broad peak at 1.5 nm.

To study the electrocatalytic activity of PAM-N-x, cyclic voltammetry (CV) was performed in 0.1 M KOH solution at a scan rate of 50 mVs^{-1} . Fig. 4 shows the cyclic voltammograms of the PAM-N-x samples. For all samples, the CV curves measured in O_2 -saturated electrolyte show a reduction peak at ~0.88 V (vs. RHE), indicating the intrinsic ORR activity of PAM-N-x samples. To further evaluate the ORR activity of PAM-N-x samples, linear sweep voltammetry was measured on a rotating disk electrode (RDE). The RDE measurements were performed in O_2 -saturated 0.1 M KOH solution with a potential scan rate of 5 mV s^{-1} under a rotation speed of 1600 rpm. As shown in Fig. 5, the LSV curve of the PAM-N-0.41 sample exhibits the highest catalytic performance for the ORR, with an onset potential and diffusion limiting current of 1.04 V (vs. Hg/HgO) and 5.34 mA cm^{-2} , respectively, which surpasses that of the Pt/C catalyst.

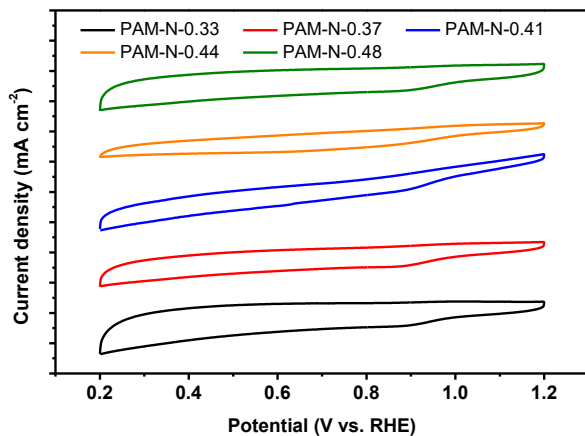


Figure 4. CV curves of PAM-N-x samples in O_2 -saturated 0.1 M KOH with a scan rate of 50 mVs^{-1}

The enhanced ORR activity could be ascribed to doped nitrogen atoms can improve the electron density of the carbon matrix and facilitate the ORR[18]. Several reports indicated that pyridinic-N and graphitic-N are active sites for the ORR, and pyrrolic-N shows no activity towards the ORR[35-38]. In our case, the PAM-N-0.41 sample possesses the most optimized N/C ratio, which serves enough active sites and transport channels for oxygen and electrolyte and has the best electrocatalytic ability for the ORR. However, the ORR activity of PAM-N-x catalysts decreases with further increases in nitrogen content. Remarkably, this trend suggests that doped nitrogen content

should not be the sole factor in determining the activity of catalysts for the ORR. The results shown in Table 2 for the synthesis of PAM-N-x from polyacrylamide hydrogel precursors indicate that the N/C ratio used in synthesis not only affects the actual N content and type but also affects the actual BET area of the final catalysts. The catalysts prepared using high N/C ratios display high surface N/C ratios but lower surface areas. PAM-N-0.48 possesses the highest surface N/C ratio but the lowest surface areas, resulting in catalysts with fewer accessible N sites. Accordingly, the optimized N/C ratio during the synthesis of the samples results in catalysts with more accessible N sites, and thus more active catalysts for the ORR are obtained.

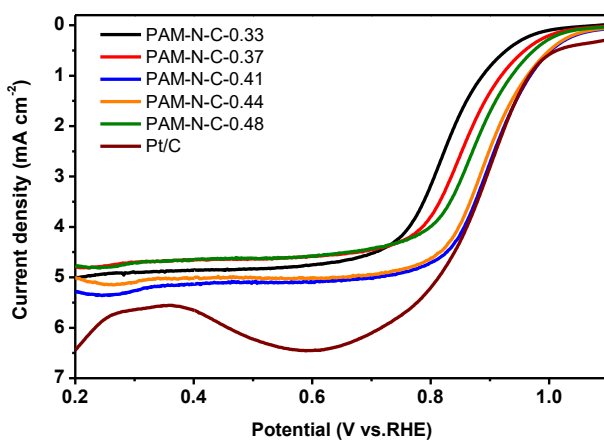


Figure 5. LSV curves of PAM-N-x samples at a rotation rate of 1600 rpm in O₂-saturated 0.1 M KOH solution with a scan speed of 5 mV s⁻¹

RDE measurements at various rotating speeds from 400 to 2000 rpm with a scan rate of 5 mV s⁻¹ were performed to investigate the reaction pathway of PAM-N-0.41 during the ORR (Fig. 6a), and its corresponding Tafel slope was also calculated (Fig. 6b). The results show a similar Tafel slope for PAM-N-0.41 (68.2 mV per decade) and Pt/C (67.8 mV per decade), indicating that the transfer of the first electron is likely the rate-determining step in the ORR for PAM-N-0.41, similar to platinum-based materials[39]. The kinetics were studied by Koutecky-Levich (K-L) plots and the transferred electron numbers of PAM-N-0.41 were calculated with the Koutecky-Levich equation (Fig. 6c). The n value ranged from 3.63 to 3.97, suggesting the PAM-N-0.41 sample catalyzes the ORR through a quasi-four-electron process.

The durability of the catalysts towards the ORR is of great significance for practical application in fuel cells. In this study, the durability of PAM-N-0.41 is surveyed with chronoamperometric measurements at a constant voltage of 0.6 V for 20000 s in 0.1 M KOH aqueous solution saturated with O₂ at a rotation rate of 1600 rpm. The current-time (i-t) response is shown in Fig. 6d. The performance of commercial Pt/C catalyst decays rapidly, with only 73% of its initial performance retained after 20000 s. In comparison, the current retention for PAM-N-0.41 is 91% after 20000 s, indicating good stability under working conditions. These results demonstrate the potential of polyacrylamide hydrogel-derived PAM-N-0.41 catalyst for applications in fuel cells as a promising alternative for costly Pt-based electrocatalysts.

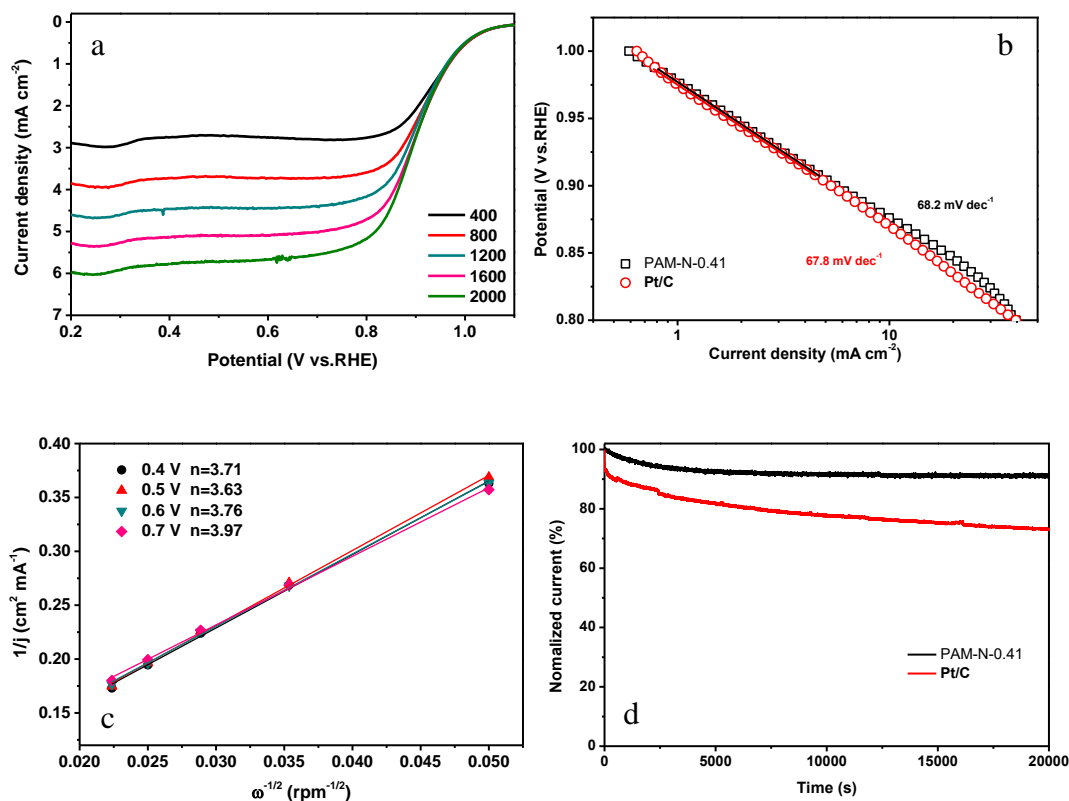


Figure 6. (a) LSVs of PAM-N-0.41 with various rotating speeds from 400 to 2000 rpm with a scan rate of 5 mV s^{-1} , (b) Tafel plots of PAM-N-0.41 and Pt/C from RDE measurements, (c) K-L plots of PAM-N-0.41 calculated from figure 6a, (d) chronoamperometric response of PAM-N-0.41 and 20wt% Pt/C for 20000 s in O_2 -saturated 0.1 M KOH at 0.6 V.

4. CONCLUSIONS

In summary, a series of nitrogen-doped microporous carbon materials with varying N/C ratios were prepared by simple pyrolysis. The characterization results show that the N/C ratio in the precursors can accommodate the nitrogen content doped in the microporous carbon to regulate the electron conductivity and catalytic performance of catalysts. Although the catalysts were prepared with high N/C ratios, they exhibit relatively low surface areas. The PAM-N-0.41 catalyst with an N/C atomic ratio of 0.41 in the precursors showed the best ORR activity in alkaline medium, which surpasses that of the Pt/C catalyst, with an onset potential and diffusion limiting current of 1.04 V (vs. Hg/HgO) and 5.34 mA cm^{-2} , respectively. The investigation shows that this type of nitrogen-doped microporous carbon material has promising potential for application in fuel cells.

ACKNOWLEDGMENTS

This work was financially supported by the National Science Foundation of China (51472034, 51404038 and 51503020) and the Doctoral Scientific Research Startup Foundation of Yangtze University (YU) (801090010137).

References

1. B. Dunn, and J. M. Tarascon, *Science*, 334 (2011) 928.
2. J. Zhang, Z. Xia, and L. Dai, *Sci. Adv.*, 1 (2015) 1500564.
3. C. Hu, and L. Dai, *Angew. Chem.*, 55 (2016) 11736.
4. R. Othman, A.L. Dicks, and Z. Zhu, *Int. J. Hydrogen Energy*, 37 (2012) 357.
5. J. Wu, and H. Yang, *Acc. Chem. Res.*, 46 (2013) 1848.
6. L. Dai, Y. Xue, L. Qu, H.J. Choi, and J.B. Baek, *Chem. Rev.*, 115 (2015) 4823.
7. S.N.S. Goubert-Renaudin, and A. Wieckowski, *J. Electroanal. Chem.*, 652 (2011) 44.
8. Z. Xia, L. An, P. Chen, and D. Xia, *Adv. Energy Mater.*, 6 (2016) 1600458.
9. X. Wang, S.I. Choi, L.T. Roling, M. Luo, C. Ma, L. Zhang, M. Chi, J. Liu, Z. Xie, J.A. Herron, M. Mavrikakis, and Y. Xia, *Nat. Commun.*, 6 (2015) 7594.
10. R. Ferrando, J. Jellinek, and R.L. Johnston, *Chem. Rev.*, 108 (2008) 845.
11. B. L. Chen, R. Li, G.P. Ma, X.L. Gou, Y.Q. Zhu, and Y.D. Xia, *Nanoscale*, 7 (2015) 20674.
12. H. Zhu, S. Zhang, Y.X. Huang, L. Wu, and S. Sun, *Nano Lett.*, 13 (2013) 2947.
13. Y. Xu, W. Bian, J. Wu, J.H. Tian, and R. Yang, *Electrochim. Acta*, 151 (2015) 276.
14. S.C. Cai, Z.H. Meng, H.L. Tang, Y. Wang, P. Tsiakaras, *Appl. Catal. B*, 217(2017)477.
15. F. He, X. Chen, Y. Shen, Y. Li, A. Liu, S. Liu, T. Mori, and Y. Zhang, *J. Mater. Chem., A* 4 (2016) 6630.
16. Z. Liu, F. Peng, H. Wang, H. Yu, W. Zheng, and J. Yang, *Angew. Chem.*, 50 (2011) 3315.
17. L. Yang, S. Jiang, Y. Zhao, L. Zhu, S. Chen, X. Wang, Q. Wu, J. Ma, Y. Ma, and Z. Hu, *Angew. Chem.*, 50 (2011) 7270.
18. K. Gong, F. Du, Z. Xia, M. Durstock, and L. Dai, *Science*, 323 (2009) 760.
19. J. Shi, X. Zhou, P. Xu, J. Qiao, Z. Chen, and Y. Liu, *Electrochim. Acta*, 145 (2014) 259.
20. X. Zhao, H. Zhao, T. Zhang, X. Yan, Y. Yuan, H. Zhang, H. Zhao, D. Zhang, G. Zhu, and X. Yao, *J. Mater. Chem. A*, 2 (2014) 11666.
21. J. Shui, M. Wang, D. Feng, and L. Dai, *Sci. Adv.*, 1 (2015) e1400129.
22. W. Xia, J. Masa, M. Bron, W. Schuhmann, and M. Muhler, *Electrochim. Commun.*, 13 (2011) 593.
23. X. Yuan, X.L. Ding, C.Y. Wang, and Z.F. Ma, *Energy Environ. Sci.*, 6 (2013) 1105.
24. Y. Li, H. Zhang, Y. Wang, P. Liu, H. Yang, X. Yao, D. Wang, Z. Tang, and H. Zhao, *Energy Environ. Sci.*, 7 (2014) 3720.
25. X. Liu, L. Li, W. Zhou, Y. Zhou, W. Niu, and S. Chen, *Chemelectrochem*, 2 (2015) 803.
26. W. Yang, T.P. Fellinger, and M. Antonietti, *J. Am. Chem. Soc.*, 133 (2011) 206.
27. H. Liang, X. Zhuang, S. Brüller, X. Feng, and K. Müllen, *Nat. Commun.*, 5 (2014) 4973.
28. H. Wu, L. Shi, J. Lei, D. Liu, D. Qu, Z. Xie, X. Du, P. Yang, X. Hu, J. Li, and H. Tang, *J. Power Sources*, 323 (2016) 90.
29. J.R. Pels, F. Kapteijn, J.A. Moulijn, Q. Zhu, and K.M. Thomas, *Carbon*, 33 (1995) 1641.
30. D.S. Su, J. Zhang, B. Frank, A. Thomas, X. Wang, J. Paraknowitsch, and R. Schlögl, *Chemsuschem*, 3 (2010) 169.
31. H. Kim, K. Lee, S.I. Woo, and Y. Jung, *Phys. Chem. Chem. Phys.*, 13 (2011) 17505.
32. S. Gao, K. Geng, H. Liu, X. Wei, M. Zhang, P. Wang, and J. Wang, *Energy Environ. Sci.*, 8 (2014) 221.
33. C. Domínguez, F.J. Pérez-Alonso, M.A. Salam, S.A. AlThabaiti, M.A. Peña, and L.B.S. Rojas, *J. Mater. Chem., A* 3 (2015) 24487.
34. F. Jaouen, J. Herranz, M. Lefevre, J.P. Dodelet, U.I. Kramm, I. Herrmann, P. Bog-danoff, J. Maruyama, T. Nagaoka, A. Garsuch, J.R. Dahn, T. Olson, S. Pylypenko, P. Atanassov, and E.A. Ustinov, *Acs Appl. Mater. Interfaces*, 1 (2009) 1623.
35. W. He, C. Jiang, J. Wang, and L. Lu, *Angew. Chem.*, 53 (2014) 9503.
36. Q. Li, B.W. Noffke, Y. Wang, B. Menezes, D.G. Peters, K. Raghavachari, and L.S. Li, *J. Am. Chem. Soc.*, 136 (2014) 3358.

37. T. Sharifi, G. Hu, X. Jia, and T. Wagberg, *Acs Nano*, **6** (2012) 8904.
38. S. Yasuda, L. Yu, J. Kim, and K. Murakoshi, *Chem. Commun.*, **49** (2013) 9627.
39. Z. Shao, L. Tong, Y. Qian, R. Dun, and W. Li, *Rsc Adv.*, **7** (2017) 39178.

© 2018 The Authors. Published by ESG (www.electrochemsci.org). This article is an open access article distributed under the terms and conditions of the Creative Commons Attribution license (<http://creativecommons.org/licenses/by/4.0/>).